Available online at www.sciencedirect.com
ScienceDirect
Journal of Nuclear Materials 363–365 (2007) 1323–1328
journal of nuclear materials
www.elsevier.com/locate/jnucmat

ICRF long-pulse discharge and interaction with a chamber wall and antennas in LHD

K. Saito [a,*], T. Mutoh [a], R. Kumazawa [a], T. Seki [a], Y. Nakamura [a], N. Ashikawa [a], K. Sato [a], M. Shoji [a], S. Masuzaki [a], T. Watari [a], H. Ogawa [b], H. Takeuchi [c], H. Kasahara [a], F. Shimpo [a], G. Nomura [a], M. Yokota [a], C. Takahashi [a], A. Komori [a], Y. Zhao [d], J.S. Yoon [e], J.G. Kwak [e], The LHD Experimental Group

[a] *National Institute for Fusion Science, 322-6 Oroshi, Toki, Japan*
[b] *Graduate University for Advanced Studies, Hayama, Japan*
[c] *Nagoya University, Nagoya, Japan*
[d] *Institute of Plasma Physics, Chinese Academy of Science, Hefei, People's Republic of China*
[e] *Korea Atomic Energy Research Institute, Daejeon, Republic of Korea*

Abstract

During long-pulse discharges by minority ion cyclotron range of frequencies (ICRF) heating (majority: He^{++} and minority: H^{+}) in the large helical device (LHD), phenomena of hot spots on antenna side protectors, localized divertor plate temperature increase and sparks from inner side of torus were observed. Plasma duration time was limited by the gradual or sudden density increase. The gradual density increase was due to outgassing from the graphite divertor plates or antenna side protectors with hot spots. The spark resulted in sudden density increase. It is thought that the localized divertor plate temperature increase and sparks are attributed to the high-energy ions accelerated in front of ICRF antennas. By suppressing these phenomena the world largest input energy was achieved.

PACS: 52.40.Fd; 52.40.Hf; 52.50.Qt

Keywords: ICRF; LHD; Outgassing; RF; Steady state

1. Introduction

In the long-pulse operation there are several issues, e.g., the heat removal, the particle control and the impurity penetration etc. [1–3]. When RF power source is employed as a plasma heating, RF sheath potential enhances plasma heat load and subsequent impurity penetration [4,5]. The large helical device (LHD) [6,7] is suitable for steady-state plasma discharge operation, because it does not require a plasma current in order to confine plasma. Three heating systems are installed in the LHD: neutral beam injection (NBI) heating, electron cyclotron heating (ECH), and ion cyclotron range

* Corresponding author.
E-mail address: saito@nifs.ac.jp (K. Saito).

0022-3115/$ - see front matter © 2007 Elsevier B.V. All rights reserved.
doi:10.1016/j.jnucmat.2007.01.269

of frequencies (ICRF) heating. A high-power ICRF heating system was developed for the purpose of long-pulse plasma operation [8–10]. High power and long-pulse plasma was possible only by ICRF heating in LHD and the input energy reached to 1.6 GJ by this heating system, which was the world record. In the ICRF heating system, two pairs of ICRF loop antennas were used in the LHD and the antenna straps were perpendicular to the toroidal direction in order to launch the fast wave. RF power was fed into the ICRF antennas from the upper and lower ports of the LHD. Graphite side protectors are attached on both sides of each antenna to protect it against the plasma heat load. The antennas are movable in the radial direction so that the distance between the antennas and the last closed flux surface (LCFS) could be changed. In the LHD, helium is used as the majority ion and hydrogen as the minority for minority ion heating. In a previous study, a high heating efficiency (absorbed power/injected power) of 80% was obtained by the minority ion heating at a frequency of 38.47 MHz, and the magnetic field strength on axis B_{ax} of 2.75 T [11]. The ion cyclotron resonance layers were located near the saddle point, where the gradient of the magnetic field strength was small; therefore, strong absorption was expected and the best heating performance has been achieved. The plasma with stored energy of 240 kJ was achieved only with an ICRF power of 2.3 MW [12]. Therefore, the long-pulse experiment has been conducted by using the minority ion ICRF heating with this position of the ion cyclotron resonance layer. However, plasmas were often terminated due to radiation collapse accompanied by the density increase. In the case of ICRF heating in LHD, the density limit is approximately n_e $[10^{19}\,m^{-3}] = 1.4 \times P_{input}$ [MW] under input power of 1.3 MW [13]. To minimize the increase in density is the major subject in LHD steady-state operation.

In Section 2, we discuss the hot spots that emerged on the antennas during long-pulse discharges. The cause of plasma collapse is discussed in Section 3. In Section 4 are described the results of a long-pulse discharge of the input energy of 1.6 GJ, which was achieved in experiments conducted in 2006. Section 5 is a summary.

2. Hot spots on the ICRF antennas

Hot spots were observed by CCD cameras during long-pulse operation on two ICRF antennas (3.5U and 7.5U) in the same position at the top of the left side protectors attached to the upper antennas. For the 7.5U antenna, an infrared (IR) camera was installed to measure the temperature of the antenna. Fig. 1(a) is a drawing of the antenna showing the graphite side protectors installed on each side and Faraday shield. Fig. 1(b) shows the temperature distribution on the antenna measured by the IR camera. In the pre-experiment of applying RF power in the vacuum condition the antenna was not heated in this position, nor was it heated in the case of the plasma discharge by NBI only. Therefore, the appearance of hot spots is related to the plasma and the RF field by ICRF antennas. Additionally, the position of the hot spot did not shift when magnetic field strength was changed to $B = 1.375$ T, 1.5 T, 2.5 T and 2.75 T. Thus, the position of hot spot was thought to be independent of the position of the ion cyclotron resonance layer. Therefore the mechanism of hot spot formation is not related to the high-energy particles created by ICRF antennas. Possible cause is the RF sheath. The temperature of the hot spot decreased with increasing in the distance Δ between the antenna and the LCFS. Fig. 2 shows the time evolution of the temperature of the hot spot. The conditions of the two plasma

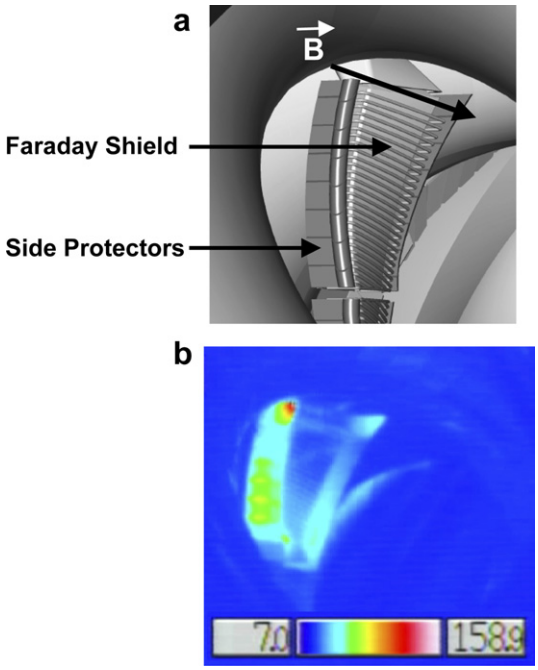

Fig. 1. (a) Drawing of 7.5U ICRF antenna. Magnetic field line is along the Faraday shield as shown by the arrow. (b) Temperature distribution of the ICRF antenna. A hot spot was observed on the top of the left side protector.

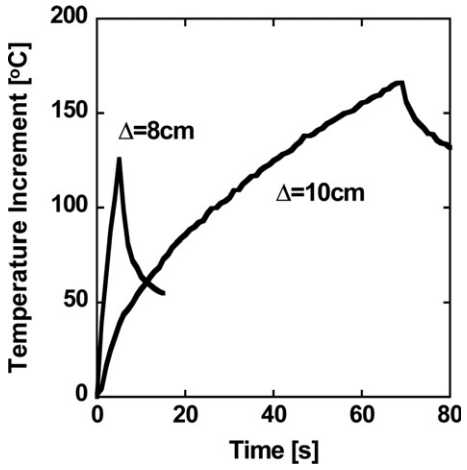

Fig. 2. Decrease in the temperature of the hot spot with respect to the large distance between the antenna and the last closed flux surface. Pulse duration times were 5 s for $\Delta = 8$ cm and 70 s for $\Delta = 10$ cm.

discharges were identical except for the distance Δ and the duration time. The line-averaged electron density was 0.7×10^{19} m^{-3} and the major radius and magnetic field strength on the axis were set at $R_{ax} = 3.55$ m and $B_{ax} = 2.789$ T, respectively. The input power of the 7.5U antenna was 250 kW. When the distance Δ was changed from 8 cm to 10 cm, the temperature rise was drastically mitigated. In the long-pulse plasma discharges antennas were located at the farthest position from the plasma in order to decrease the temperature. The relation between Δ and the hot spot temperature is reasonable since the heat flux by the RF sheath increase with electron density and electron and ion temperatures. In the case of steady-state condition the heat load q can be estimated as

$$q = \lambda \frac{\Delta T}{l} S,$$

where λ is the heat conductivity of graphite, ΔT is the temperature deference between the heat sink and the hot spot. The distance from the hot spot to the heat sink is l and cross section of the protector is S. In the case of $\Delta T = 900$ °C, which was observed during the discharge of 1.6 GJ input energy, the heat load can be calculated to be 300 W.

3. The causes of plasma collapse

In the LHD, the duration time of plasma sustained by ICRF heating had previously been limited because of radiation collapse accompanied by a gradual and uncontrollable increase in density due to outgassing [14]. This phenomenon was seen in the early phase of long-pulse discharge experiment in 2006, but the outgassing was reduced by the aging of graphite divertor plates and antenna side protectors with hot spots, which were thought to be the source of outgassing, with repeating the discharges. The temperature rise in the divertor plates at inner side of the torus was large when the major radius of magnetic axis was employed at 3.6 m and it became large in the divertor plates located at bottom and top of the torus when the major radius of the magnetic axis was 3.75 m. However, when the magnetic axis was located at the vicinity of 3.68 m, the temperature increase in their divertor plates was kept low [15]. Setting the magnetic axis on this optimal major radius and sweeping the radius of magnetic axis have also been found to be useful in dispersing the localized heat load and reducing the outgassing from the divertor plates.

We also experienced another kind of the plasma collapse in which the electron density increased abruptly and the plasma collapsed due to the increase in the radiation power. It was found that the hot spot on the antenna has no relation with this abrupt increase in the radiation power. Fig. 3 shows the relation between the plasma duration time and antenna plasma distance. Distance Δ is used as the indication of temperature on the hot spot because the temperature surpassed the upper limit of measurement (1100 °C). Smaller distance Δ means higher temperature but duration time was not decreased by decreasing Δ. One of causes of the abrupt density increase was thought to be the injection of impurities into the plasma by sparks from the inner side of torus, because in several discharges

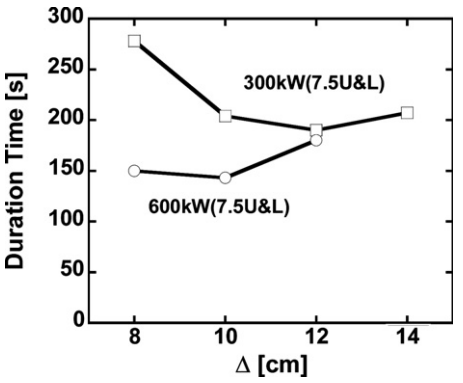

Fig. 3. Relation between antenna position and plasma duration time.

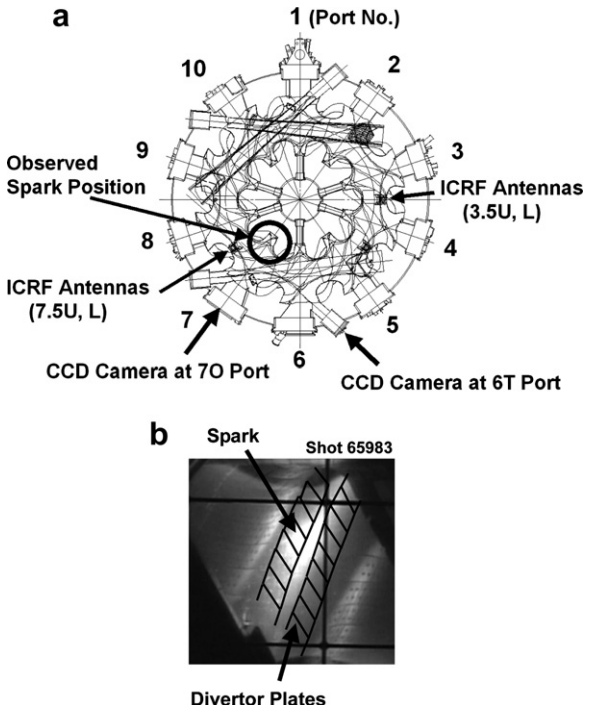

Fig. 4. (a) Top view of LHD. Sparks were observed by two CCD cameras. (b) A spark from inner side of a torus seen by the CCD camera installed in 7O port. It seems that the spark came from near the left side of divertor plates.

sparks were seen by the CCD camera installed in 7O port as shown in Fig. 4(a) and (b). This toroidal position of spark relative to 7.5U and L antennas was the same with local enhanced divertor plate temperature. It seems that the spark came from near the left side of divertor plates. Fig. 5(a) shows another spark seen by the CCD camera installed in 6 T port. The time evolution of the plasma parameters at the timing of the spark is shown in Fig. 5(b). FeX intensity is measured in 7O port. Normally an increase in the FeX intensity was not observed at the end of discharge, but in the case of the abrupt plasma collapse, it was observed as shown in the bottom graph of Fig. 5(b). Therefore, Fe injection by the spark was thought to be main cause of the collapse. Even the small sparks were not seen initially and this phenomenon is therefore thought to be closely related to the temperature increment of the chamber wall including the divertor plates. In the case of the minority ion heating, accelerated protons at the cyclotron resonance layer out of the LCFS in front of the antennas can be the cause of the localized temperature distribution in the toroidal direction [14]. Therefore, the high-energy hydrogen ion in the peripheral region of the plasma is thought to be the possible

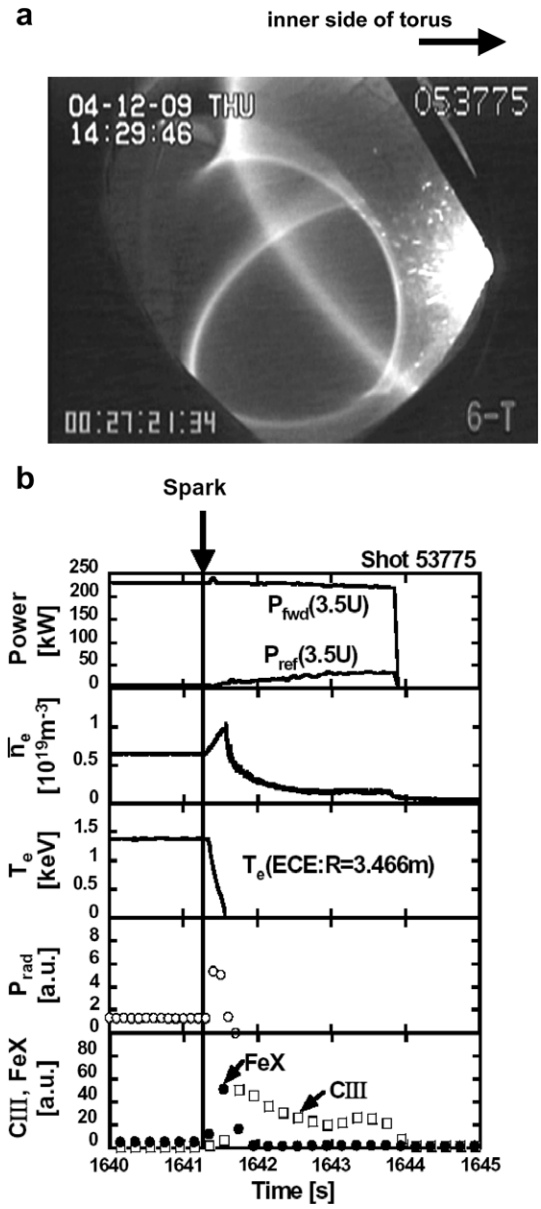

Fig. 5. (a) A spark observed on the inner side of a torus seen by the CCD camera installed in 6 T port. (b) Time evolution of plasma parameters at the termination of plasma by the spark.

cause of sparks. The other cause of the abrupt density increase was thought to be the spark of antenna-wall arcing because there was a mark of the arcing. This problem will be solved by widening the antenna-wall gap.

4. Achievement of 1.6 GJ input energy discharge

The duration time is plotted against the input power as shown in Fig. 6(a). In a high-power

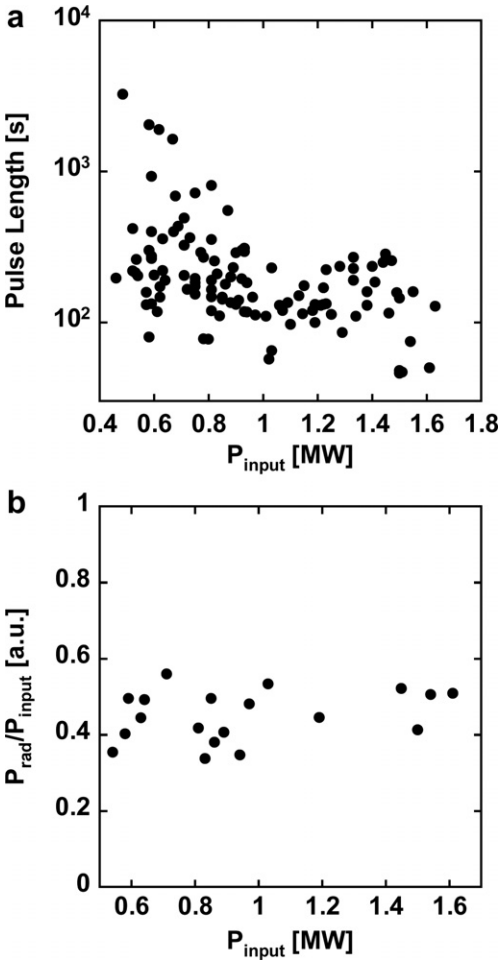

Fig. 6. (a) Relationship between input power and pulse length. (b) Relationship between input power and radiation power normalized by input power at the timing of collapses.

discharge with more than 1 MW, the duration time of 4 min and 45 s at an ICRF heating power of 1.3 MW and ECH power of 0.1 MW was achieved. However, the plasma collapsed due to the abrupt density increase. We could not extend the duration time more than 5 min with the heating power of over 1 MW because intense sparks, which result in the radiation collapse due to the abrupt density increase, occurred frequently with increasing in heating power. Fig. 6(b) shows the relationship between input power and radiation power at the time of plasma collapse normalized by input power. It seems that plasma collapses when the normalized radiation power reaches a threshold. To prevent frequent and intense sparks, we lowered the ICRF power for the extension of the duration time. To maintain the plasma for a long time, a method to adjust the ICRF heating power from each antenna with monitoring sparks were also tried for the first time. Using this technique, a plasma discharge of 54 min and 28 s was achieved with ICRF heating supported by ECH. Fig. 7 shows the time evolutions of various parameters of the plasma discharge, which was the longest duration time in the plasma discharges using the ICRF heating. In this discharge, three ICRF antennas (3.5U and 7.5U, L antennas) were used. The initial ICRF heating power was 600 kW, but from 100 s it was gradually decreased by a manual control in order to reduce the frequent sparks. At 400 s power of 7.5L antenna was turned off. Then divertor plate temperature at 7.5L port and wall temperature at 7I port were decreased and frequent sparks seen around 7I port were suppressed. The sudden decrease in the ICRF heating power measured at 1600 s was caused by a problem in an impedance matching device. This problem was solved at 2000 s and the power was carefully increased while sparks were monitored. The averaged injection powers of ICRF heating

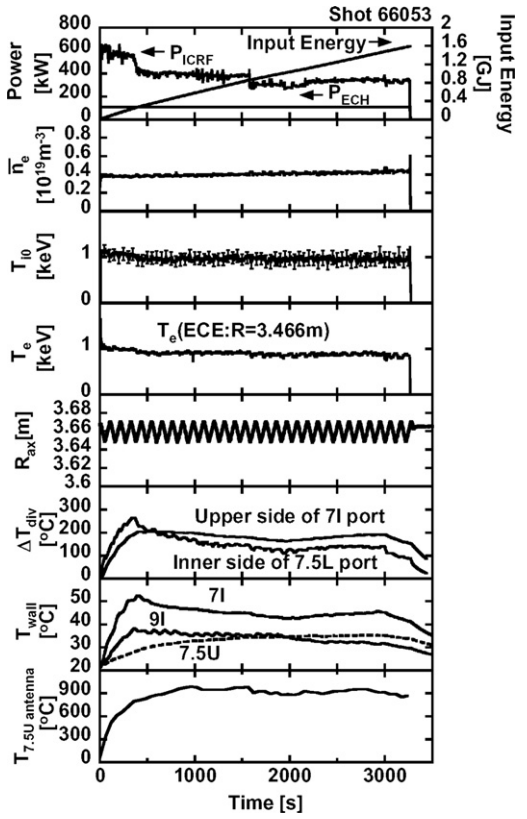

Fig. 7. Longest pulse discharge of ICRF heated plasma in LHD. The total input energy reached 1.6 GJ.

and ECH were 377 kW and 110 kW, respectively. The total injected energy reached 1.6 GJ, surpassing the previous record of 1.3 GJ established in 2004 [15–17]. The ion and electron temperatures on the magnetic axis were approximately 1 keV. The line-averaged electron density was maintained at 0.4×10^{19} m^{-3} by the feedback control of gas puffing. The major radius of magnetic axis was swept from 3.65 m to 3.67 m to reduce the local intense plasma heat load on the divertor plates. The hot spot on the 7.5U antenna was seen, but the temperature was saturated at 900 °C. This discharge collapsed due to the abrupt density increase. An increase in FeX intensity was also observed. Therefore we think the influx of iron by sparks, which were unfortunately not observed by the existing cameras, is possible cause of plasma collapse.

5. Summary

During the long-pulse discharge a hot spot was observed on the top of the ICRF antenna side protector, which was thought to be caused by RF sheath. Localized divertor plate temperature increase and sparks from inner side of torus were also observed. The hot spot and localized divertor plate temperature increase are possible cause of radiation collapse with gradual density increase by outgassing. On the other hand spark terminates plasma with the abrupt radiation power increase. High-energy ion flux accelerated near ICRF antenna are plausible cause of localized divertor plate temperature increase and sparks from inner side of torus.

Gradual density increase was overcome by the aging of divertor plates and antenna side limiters with hot spots by operating a number of plasma discharges. Sweeping the major radius of the magnetic axis around the proper position also contributed to decrease outgas from divertor plates. The problem in the long-pulse plasma operation with the high ICRF power, e.g., more than 1 MW still remains, however, suppressing of sparks by a control of the ICRF heating power enabled the achievement of the world largest input energy of 1.6 GJ.

Acknowledgements

The authors would like to thank the technical staff of the LHD group of the National Institute for Fusion Science for their helpful support during this work. This work was supported in part by NIFS budget NIFS05ULRR504-508 and the JSPS-CAS Core-University Program in the field of 'Plasma and Nuclear Fusion'.

References

[1] H. Zushi et al., Nucl. Fusion 41 (2001) 1483.
[2] D. van Houtte et al., Nucl. Fusion 44 (2004) L11.
[3] X. Gao et al., J. Nucl. Mater. 337–339 (2005) 835.
[4] D.A. D'Ippolito et al., Nucl. Fusion 42 (2002) 1357.
[5] L. Colas et al., Nucl. Fusion 43 (2003) 1.
[6] A. Komori et al., Plasma Phys. Control. Fusion 45 (2003) 671.
[7] O. Motojima et al., Fusion Sci. Technol. 46 (2004) 1.
[8] R. Kumazawa et al., Proc. 19th Symp. Fusion Technol. 1 (1996) 617.
[9] T. Mutoh et al., J. Plasma Fusion Res. SERIES 1 (1998) 334.
[10] T. Seki et al., Fusion Sci. Technol. 40 (2001) 253.
[11] K. Saito et al., Nucl. Fusion 41 (2001) 1021.
[12] T. Seki et al., Proc. 14th Top. Conf. RF Power Plasmas 595 (2001) 67.
[13] R. Kumazawa et al., Phys. Plasmas 8 (2002) 2139.
[14] K. Saito et al., J. Nucl. Mater. 337–339 (2005) 995.
[15] Y. Nakamura et al., Nucl. Fusion 46 (2006) 714.
[16] T. Mutoh et al., J. Plasma Fusion Res. 81 (4) (2005) 229.
[17] R. Kumazawa et al., Nucl. Fusion 46 (2006) S13.